Spatial Scales of Sea Surface Salinity Subfootprint Variability in the SPURS Regions

Frederick M. Bingham[1]* and Zhijin Li[2]

[1] University of North Carolina Wilmington, Department of Physics & Physical Oceanography; binghamf@uncw.edu

* Correspondence: binghamf@uncw.edu

[2] Jet Propulsion Laboratory, California Institute of Technology; zhijin@jpl.nasa.gov

Abstract: Subfootprint variability (SFV), or representativeness error, is variability within the footprint of a satellite that can impact validation done by comparison of in situ and remote sensing data. This study seeks to determine the size of the SFV as a function of footprint size in two regions that were heavily sampled with in situ data. The SPURS-1 (Salinity Processes in the Upper-ocean Regional Studies) experiment was conducted in the subtropical North Atlantic in 2012-2013, whereas the SPURS-2 study was in the tropical eastern North Pacific in 2016-2017. SFV was also computed using a high-resolution regional model based on ROMS (Regional Ocean Modeling System). We computed SFV at footprint sizes ranging from 20-100 km for both regions. SFV is strongly seasonal, but for different reasons in the two regions. In the SPURS-1 region, the meso- and submesoscale variability seemed to control the size of the SFV. In the SPURS-2 region, the SFV is much larger than SPURS-1 and controlled by patchy rainfall.

Keywords: surface salinity, remote sensing, subfootprint variability, representativeness error, spatial scale

1. Introduction

Sea surface salinity (SSS) has been measured by satellite for over 10 years from three different platforms, ESA's SMOS (Soil Moisture and Ocean Salinity), NASA and CONAE's Aquarius and NASA's SMAP (Soil Moisture Active Passive). The value of these measurements to the scientific community and for practical applications has become clear over this time as has the need for continuity. SMOS has been aloft since 2009 and, though still returning good data, is long past its expected lifetime. Aquarius stopped transmitting in 2015. SMAP, also still returning good data, is having to rely on ancillary measurements of sea surface roughness because its onboard scatterometer stopped functioning soon after launch. Given all of this, there has been much interest in developing new missions to measure SSS, and thus the need to understand the parameters of a such a mission.

Subfootprint variability (SFV) is the variance within the footprint of a satellite measurement [1-3]. Because satellite SSS measurements are areal averages over a relatively large footprint (e.g. [4]), and because validation is carried out by comparison to in situ data [5-8], there is a mismatch that can introduce error into the validation process as explained in detail by [1]. The size of this error is beginning to be understood [1-3,9]. However, these important previous studies

46 have been based on the footprint the size of Aquarius, 100 km, whereas the SMAP
47 and SMOS missions have smaller footprints. The amount of SFV should depend on
48 the size of the footprint, as well as many other factors such as season, geographic
49 location and the strength of mesoscale and submesoscale stirring of the SSS field.
50   One of the most interesting results that has come out of the increased
51 measurement of SSS over the past decade is on the spatial scales of variability.
52 While other surface variables measured by satellite, namely sea surface
53 temperature (SST) and sea surface height (SSH), have relatively large scales [10-12],
54 SSS variability occurs on a smaller scale [13]. To quantify this, using numerical
55 model output focusing on the western North Pacific and Arabian Sea, [14] found
56 that about 50% of open ocean SSS variance in these regions is on a scale of 50 km or
57 less. That is, most ocean variance occurs on a scale that is smaller than the footprint
58 of Aquarius, and of similar size to that of SMAP.
59   This paper is an extension of [1], who assumed the footprint size to be a
60 constant 100 km. In the present work, we explore how SFV depends on footprint
61 size, and get some idea of what exactly causes SFV. The approach is to look at two
62 heavily sampled regions, a couple of the small number places in the ocean where
63 SFV can be reliably determined using in situ data. The picture here is that SFV can
64 be roughly divided into 4 causes: (1) rainfall-induced fresh patches (e.g. [15]); (2)
65 internal ocean submesoscale and mesoscale variability; (3) large-scale fronts such
66 as the North Equatorial Countercurrent (NECC) front that moves between the
67 equator and 10°N and (4) mean gradients. These 4 causes are ordered roughly in
68 terms of scale from smallest to largest.
69   The two regions we are studying are SPURS-1 (Salinity Processes in the Upper
70 Ocean Regional Study – 1) and SPURS-2. SPURS-1 is a field campaign that took
71 place in the subtropical North Atlantic in 2012-2013 ([16] and references therein)
72 centered on a mooring at (24.5°N,38°W). The SPURS-1 region is evaporation-
73 dominated with small gradients and weak currents. SPURS-2 took place in the
74 tropical eastern North Pacific in 2016-2017 ([17] and references therein) centered on a
75 mooring at (10°N,125°W). The SPURS-2 region is precipitation-dominated, with
76 strong currents, and falls within the intertropical convergence zone (ITCZ) for part
77 of the year [18]. See [1] Figure 3 for the locations. We expect that SFV will be induced
78 mainly by cause (2) above in the SPURS-1 region and by causes (1)-(3) in the SPURS-
79 2 region.

2. Data and Methods

81   As this work is an extension of [1], the reader is referred to section 2 of that
82 paper for a description of the data and methods used here. This paper uses the
83 same in situ data, ROMS (Regional Ocean Modeling System) output, and method
84 of computing SFV. SFV is the square root of the weighted variance within the
85 defined footprint of size $2d_0$ The only difference between the present work and [1]
86 is that the footprint size is not a constant 100 km, but is allowed to vary.
87 Additionally, in this paper, no use is explicitly made of any satellite data. A list of
88 digital object identifier (DOI) references to the datasets used in this paper is
89 included in the Acknowledgements section.
90   Brief use is made of radar-derived rainfall collected during the SPURS-2 cruise
91 in October-November 2017. The data come from the Sea-viewing Polarimetric
92 (SEA-POL) radar described by [19, 20].
93

3. Results

95 *3.1. In situ results*

96   Time series of SFV (Figure 1) in the SPURS regions indicate that it is a seasonal
97   quantity, tending to be largest in summer and fall (June-December) and smallest in
98   winter and spring (January-May). SFV in the SPURS-2 region is larger than SPURS-
99   1, though the difference is least in the low variance season. In most instances, SFV
100   is larger at the 100 km footprint size for both regions. There are isolated time
101   periods when this is reversed, especially in the SPURS-1 region. There tends to be a
102   larger distinction as a function of scale for the SPURS-1 region. That is, for SPURS-
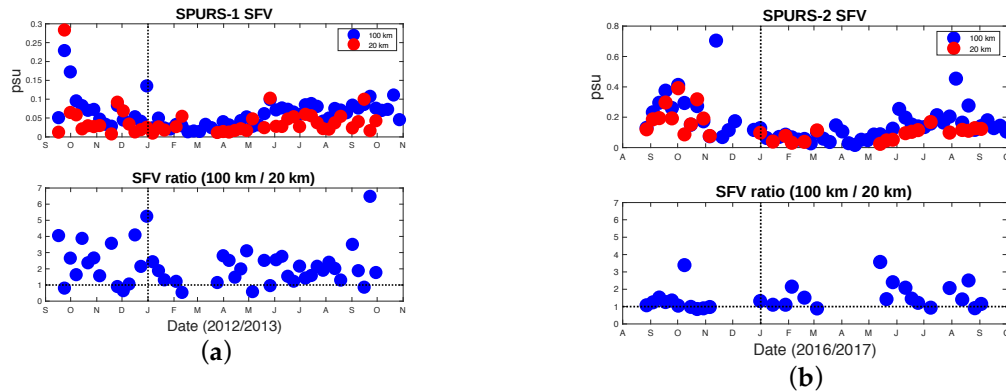103   1, the ratio of 100 km SFV to 20 km SFV is generally larger than for SPURS-2.

104   **Figure 1.** Time series of SFV in the SPURS regions. Top panels: Blue markers are SFV using a 100 km
105   footprint size. Red markers use a 20 km footprint. Bottom panels: Ratio of 100 km to 20 km SFV.
106   That is, the ratio of the blue markers in the top panels to the red markers. The horizontal dashed line
107   indicates where this ratio is 1. (**a**) SPURS-1; (**b**) SPURS-2. Note vertical axes are not consistent
108   between the top panels.

109   The findings from the time series are presented in simpler form using σ_{50}, the
110   median SFV at each site as a function of footprint size (Figure 2). As seen in Figure
111   1, SFV is as much as 4X larger at SPURS-2 than SPURS-1. At SPURS-1, SFV
112   increases with footprint size from 20 to 60 km, and then levels off at around 0.05.
113   At the SPURS-2 site, SFV does not increase at all from 20 to 60 km, and then
114   increases a little bit. There is proportionally much less dependence on footprint
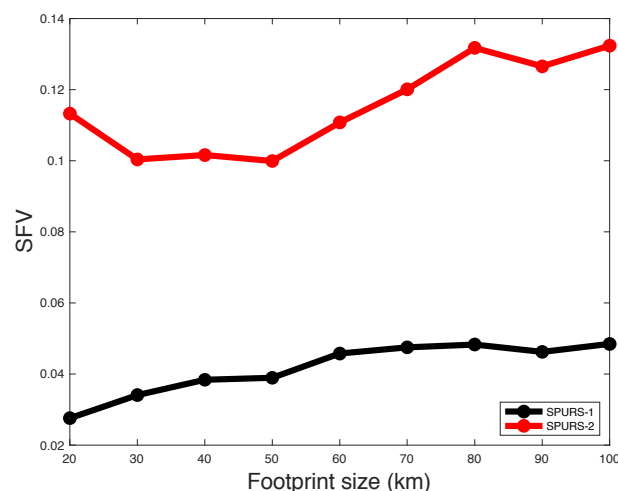115   size at SPURS-2 than SPURS-1, in agreement with Figure 1.

117   **Figure 2.** σ_{50} as a function of footprint size for SPURS-1 (black) and SPURS-2 (red) in situ data.

118   In the SPURS-1 region there is little rainfall between March 1 and August 31
119 [21], and in the SPURS-2 region between February 1 and May 31 [22]. Additionally,
120 at the SPURS-2 site, the NECC front is well south of the mooring during those
121 "dry" months [18]. So, for both sites, one can assume that any SFV there during
122 these periods is due to internal variance within the ocean and not imprinted
123 directly by the atmosphere through precipitation. Evaporation may imprint some
124 SFV, but not likely much as SSS anomalies imposed by evaporation tend to
125 dissipate quickly [23].
126   Separating the SFV out during the wet and dry periods (Figure 3), one can see
127 a sharp contrast between the regions. In the SPURS-1 region, SFV increases
128 strongly with footprint size from 20 to 70 km during the dry season, but only out to
129 40 km in the wet season. SFV is about the same between wet and dry seasons to 40
130 km. At larger footprint sizes, it is counterintuitively much larger during the dry
131 season. The dry season corresponds to spring and summer, so one has to assume
132 that internal variability is larger during these months than during fall and winter
133 at 50+ km length scales. This seems consistent with [24] who found elevated eddy
134 kinetic energy (EKE) in the SPURS-1 region during the months of April-September.
135 Larger EKE presumably means stronger eddy activity at the mesoscale, and thus
136 larger variability of SSS at that scale as well.
137   At the SPURS-2 site, the situation is very different. Wet season variability is
138 much larger than dry season. Neither season exhibits a large change with footprint
139 size, but the dry season shows almost none. Dry season median SFV is comparable
140 between the two regions at the largest (70-100 km) scales, but smaller in the
141 SPURS-1 region at smaller scales.
142   It should be noted that the dry season and the low SFV season are not the same
143 for the SPURS-1 region. The dry season is March 1 – August 31, whereas the low
144 SFV season is approximately January 1 – May 1 (Figure 1a). On the other hand, the
145 dry season and low SFV season do mostly overlap for the SPURS-2 region. This
146 suggests that there is seasonal variability inherent to the ocean at the SPURS-1 site
147 that may be more important than rainfall in determining the size of SFV. A similar
148 plot separating high SFV and low SFV seasons at the SPURS-1 site is presented in
149 Figure 4. This may be a more logical way of separating parts of the year for SPURS-
150 1, and shows the variation of SFV with scale, which is consistent between low SFV
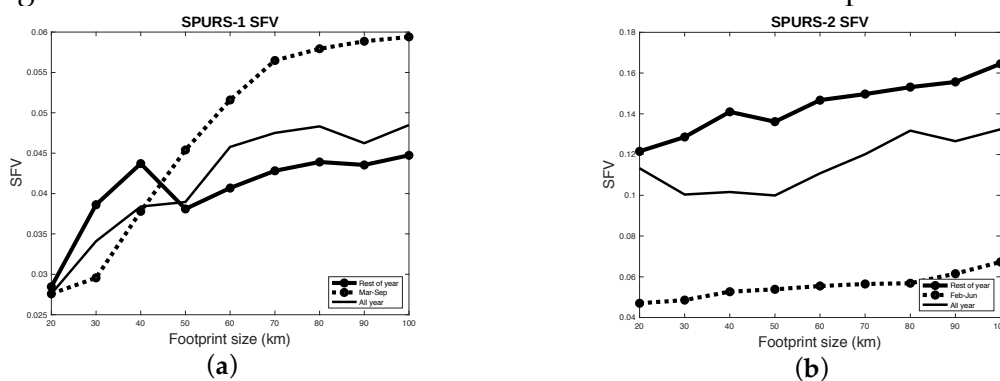151 and high SFV seasons. Both curves level off at around 70 km footprint size.

(a)   (b)

152 **Figure 3.** Median SFV vs. footprint size in the SPURS regions. Solid lines with markers: wet season.
153 Thinner solid lines with no markers: all year, same as curves shown in Figure 2. Dashed lines with
154 markers: dry season. (**a**) SPURS-1. Dry season is March 1 – August 31. (**b**) SPURS-2. Dry season is
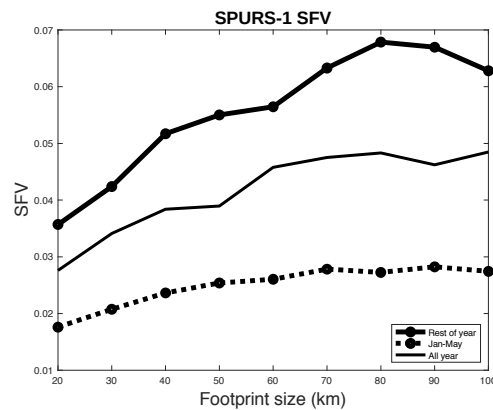155 February 1 – May 31. Note vertical axes are not consistent between the panels.

156

157   **Figure 4.** As in Figure 3a. However, the dashed line is for January 1 – May 1, and the solid line with
158   symbols is for the rest of the year.

159   In the SPURS-2 region, the fact that the wet season SFV is so much larger than
160   the dry season may be related to either (1) increased precipitation, and thus
161   imprinted small scale variability, (2) the migratory presence of the NECC front
162   during the summer and fall [18], (3) seasonally increased mesoscale variability – or
163   (4) some combination of these. Distinguishing these factors is not easy. One clue is
164   the fact that there is not much dependence of SFV on scale. If rainfall is ubiquitous
165   during these months, and it produces small fresh patches throughout the region (a
166   typical example is shown in Figure 5), and if SFV can be enhanced by even one
167   fresh patch in a given snapshot, then that argues for the importance of rainfall in
168   determining SFV. In other words, if the scale of rain-induced fresh patches is
169   smaller than the 20 km we have been studying here and most SSS variance is due
170   to these patches, then we would see little scale dependence of SFV as is the case at
171   the SPURS-2 site. It is harder to make such an argument for the NECC front. As
172   footprint size increases it has an increased probability of encompassing the front,
173   and thus should have a strong dependence on scale. The same goes for mesoscale
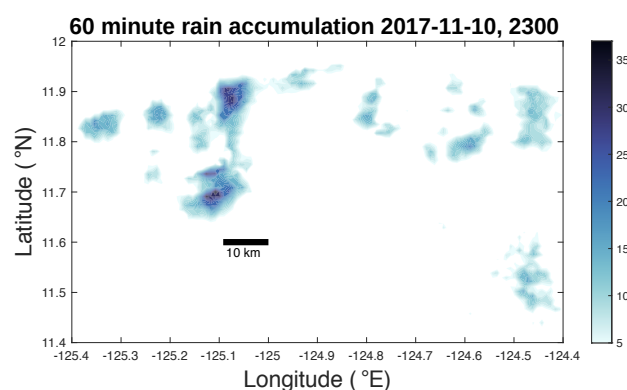174   eddies, the SFV should scale with eddy size, but does not appear to.

175

176   **Figure 5.** 60-minute rain accumulation (mm) from the SPURS-2 cruise on 11-November-2017 at
177   2300Z. No color means less than 5 mm. The data are from the SEA-POL radar used during the
178   cruise. This is a typical configuration of rainfall in the region at this time of year. A bar showing 10
179   km length is also included.

180   We can test whether SFV depends on precipitation by plotting SFV against 7-
181 day maximum rain rate (Figure 6). The scatter plots show a clear relationship
182 between rain rate and SFV even though the precipitation data used to make these
183 plots are from the SPURS central moorings, and thus may not be representative of
184 the entire footprint. So, in both regions there is evidence that rainfall plays at least
185 some role in generating SFV at a range of spatial scales. The larger the scale, the
186 greater the correlation between SFV and rainfall. Interestingly, the correlations are
187 higher for the SPURS-1 region, where rainfall is much smaller, than for the SPURS-
188 2 region. The results of Figure 3a and Figure 6a seem contradictory at first glance,
189 but one must remember that the points in Figure 6a only represent the wet season.
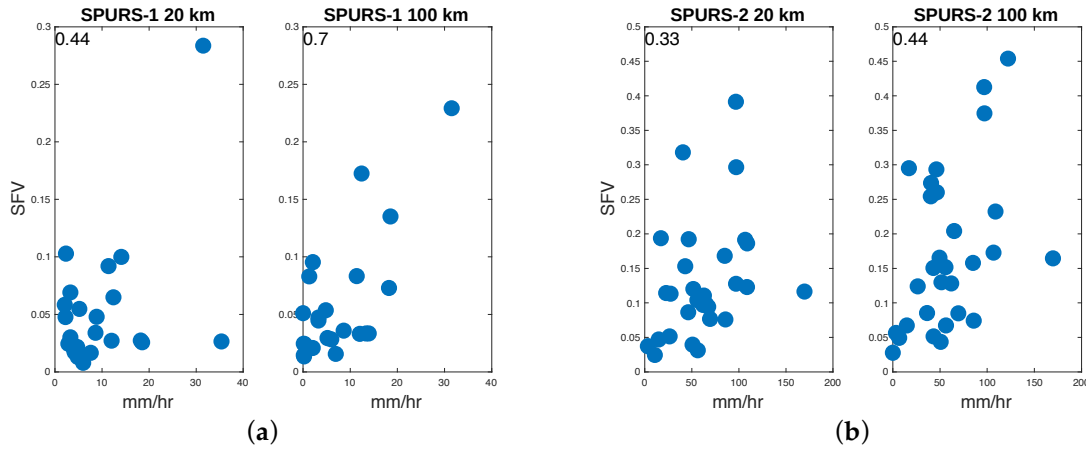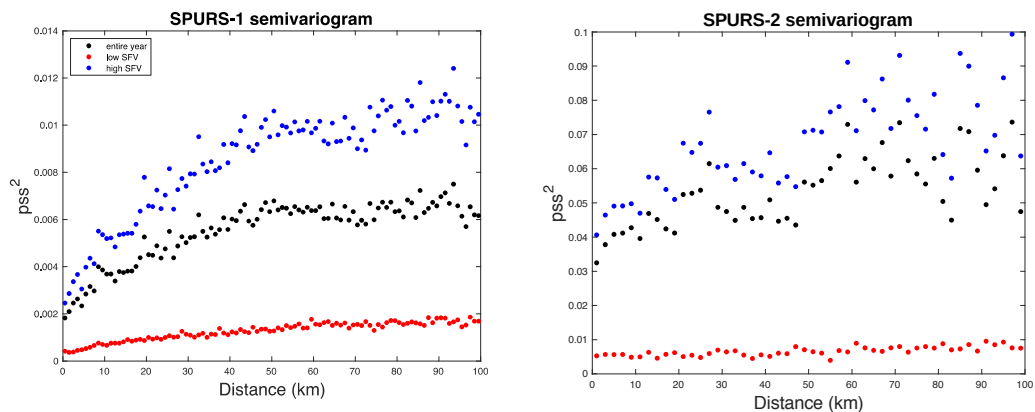190

(a)   (b)

192   **Figure 6.** SPURS SFV vs. maximum rain rate measured at the central mooring when this value
193   exceeds 2 mm/hr. Maximum rain rate was determined over the same weekly time intervals as the
194   SFV. Correlation values are shown at the top left of each panel. All are significant at the 95% level,
195   except for SPURS-1 at 20 km which is significant at the 90% level. Left panels: 20 km footprint size.
196   Right panels: 100 km footprint size. (a) SPURS-1. (b) SPURS-2. Note inconsistent axis scales between
197   (a) and (b).

198   To understand the spatial variability better, semivariograms were plotted
199 (Figure 7) using the in situ data from each site from the simple estimator [25]
200

201    $$\hat{\gamma}(v) = \frac{1}{2\,N(v)} \sum_{N(v)} \left(S(x_i) - S(x_J) \right)^2$$

202
203   Where $S(x_i)$ is the salinity at point x_i and $N(v)$ is the number of pairs of salinity
204 values where the distance between them is v.
205

(**a**)   (**b**)

206   **Figure 7.** Semivariograms as a function of distance computed from in situ data. (**a**) SPURS-1. Red
207   symbols, January 1 – May 1. Black symbols: Entire year. Blue symbols: Entire year except for
208   January 1 – May 1. (**b**) SPURS-2. Red symbols, February 1 – May 31. Black symbols: Entire year. Blue
209   symbols: Entire year except for February 1 – May 31. Note vertical axes are not consistent between
210   the panels.

211   The semivariogram shows the scales of variability. This function is closely
212   related to the spatial covariance as explained by [25]. It is the mean squared
213   difference between values as a function of spatial separation. The semivariogram
214   value at zero separation, the "nugget" in the parlance of [25], normally describes a
215   kind of instrumental error. In this case, as these values were computed using 7-day
216   snapshots, the nugget is the variance over a 7-day period.
217   The semivariograms for SPURS-1 are much as one would expect, with small
218   values at small separation, increasing to a plateau (the "sill") at 50 km or so (the
219   "range"). The semivariogram during the low SFV period is much smaller, but it
220   contains the same dependence on separation distance.
221   The semivariogram at SPURS-2 is very different. It appears to increase from 0
222   to 20 km during the wet season, reaches a plateau, and then becomes very noisy at
223   a distance beyond that. Thus, a rough estimate of the decorrelation scale is that 20
224   km. During the dry season (red symbols), though, it appears that there is almost no
225   dependence of the semivariogram on scale, because of the way the axes are
226   presented in Figure 7, it does actually increase. Despite this, there is no obvious sill
227   or range during the dry season.
228

229   *3.2. ROMS Results*

230

231   Time series of SFV computed from the ROMS (Figure 8) contrast the two
232   regions, and show the difference between model and the in situ results presented
233   in the previous section. It should be noted here that the model encompasses a
234   somewhat different time period than the in situ data collection. For SPURS-1, the
235   model covers January 1, 2012 – December 31, 2012, whereas the field campaign
236   lasted from September 2012 to September 2013, thus overlapping by 4 months. For
237   SPURS-2, the model covers February 1, 2017 – January 31, 2018, whereas the field
238   campaign went from August 2016 to November 2017, giving ~9 months of overlap.
239   The SPURS-1 model output has similar seasonality as the in situ results
240   (Figures 1 and 4). Minimum values of SFV are in February-June. The sizes match
241   more or less the ones presented in Figure 2 for 20 km footprint size, but ROMS
242   shows a larger value of SFV for 100 km footprint size than in situ, ~0.08 vs. 0.05. At
243   almost no time does the 20 km SFV exceed the 100 km as shown in Figure 1a. The
244   100 km time series is smoother than the 20 km one. Thus, the separation of SFV by
245   scale seen in the in situ data (Figure 4) is also evident in the ROMS results, but to a
246   greater degree.
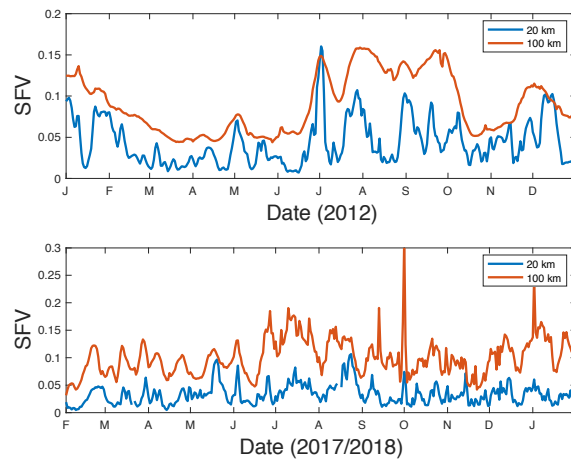247

248

249   **Figure 8.** ROMS-evaluated SFV for SPURS-1 (upper) and SPURS-2 (lower). Red (blue) curves are for
250   100 km (20 km) footprint size. Note axis scales are inconsistent between the panes.

251
252   For SPURS-2, the results are different. Values of SFV at 20 km fluctuate, but on
253   short time scales and little seasonality is evident. The 20 km SFV is much smaller
254   (~0.03) than the median in situ value of Figure 2. At 100 km, the SFV is still smaller
255   than the in situ value, ~0.1, but not by as much. Not much seasonality is evident at
256   100 km either, though SFV is slightly elevated in July-September. There is some
257   change in the time scales of variability of SFV. The time series of 100 km SFV
258   fluctuates much more rapidly after the beginning of July than before. There is a
259   clear separation of scale for the SPURS-2 region as there was for SPURS-1.
260   These results are summarized in Figure 8. Strikingly, the two curves of Figure
261   8 from the different SPURS regions are very similar in contrast to Figure 2. Both
262   show a stronger increase of SFV as a function of spatial scale than is seen in Figure
263   2. SFV at 100 km is somewhat less for SPURS-1 than SPURS-2, but they are nearly
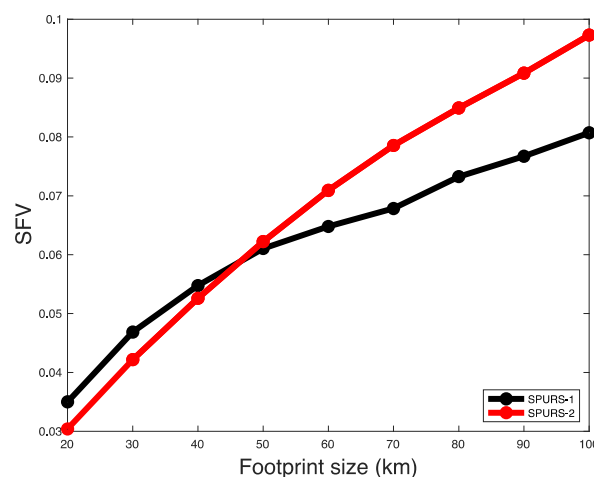264   the same at smaller scales.
265

266

267   **Figure 8.** As in Figure 2, but for ROMS output.

268
269   One of the main differences between the model and the real ocean is the
270   forcing. The ocean is forced with rainfall that occurs in small, patchy bursts,

271   especially in the SPURS-2 region (Figure 6; [19, 20, 26, 27]). These bursts create rain
272   puddles on kilometer scales [15]. ROMS is forced with 18 km NCEP (National
273   Centers for Environmental Prediction) GFS (Global Forecast System) winds and
274   precipitation [28], and thus lacks the small-scale variability in freshwater forcing
275   which could lead to large values of SFV. Perhaps this is what causes the relatively
276   small SFV and lack of seasonality in the SPURS-2 results especially at short spatial
277   scales. SFV in ROMS may be mainly a measure of ocean variability, not variability
278   imposed externally by patchy rainfall. Thus, the black curve in Figure 8 for SPURS-
279   1 is similar to the (dashed) one for the dry season in Figure 3a. There is no such
280   similarity for SPURS-2.

281   **4. Discussion**

282   We have explored SFV in two different regions and found that it varies by
283   scale differently in each place. We have used two tools to make these conclusions.
284   The first is an in situ dataset of drifters, shipboard measurements and wavegliders
285   for SPURS-1 and wavegliders only for SPURS-2 [1]. The second is high-resolution
286   regional simulations. Neither of these tools is perfect. The in situ data are not
287   comprehensive in areal and temporal coverage and contain a mixture of skin
288   surface and bulk mixed layer observations. This may be a bigger issue in the
289   SPURS-2 region because rain events produce thin shallow layers there [15, 29, 30].
290   The model lacks completely realistic forcing. It may be missing mixed-layer
291   dynamics that are important in determining or hindering the ability of fresh
292   patches to be incorporated into the bulk mixed layer and in turn affect the statistics
293   of horizontal variability, again especially in the SPURS-2 region [31].
294   Comparison of the two regions is illuminating though. In general, the SPURS-2
295   region has much higher SFV than SPURS-1 (Figure 2), as determined from in situ
296   data. (Model results are different.) Another result is that SFV in the SPURS-1
297   region has a stronger scale dependence than that of SPURS-2 (compare Figures 3b
298   and 4). The SPURS-1 SFV has clear plateaus at 60+ km in all seasons (Figures 4 and
299   7).
300   The scales of variability are straightforward to compute and interpret for
301   SPURS-1. For SPURS-2, doing this requires a more detailed analysis than has been
302   attempted here. Possibly, SSS variability is not isotropic in low latitudes and has
303   different scales in the zonal and meridional directions, though this is not the
304   conclusion of [32]. Research is ongoing into this.
305   In terms of design of future satellite missions, one can use Figures 2, 3b and 4
306   to get an idea of how much SFV to expect for a given footprint. The size of a
307   footprint is determined by the frequency of radiation being measured, the diameter
308   of the antenna, the height of the satellite above the Earth, etc., parameters which
309   can be determined in the design phase of a satellite. Though no area of the ocean is
310   the same, the two regions studied here may be thought of as typical mid-latitude
311   and tropical open ocean. The numbers displayed in Figures 2, 3b and 4 can be
312   factored into error budgets for future missions, remembering that error associated
313   with SFV is just a mismatch of scales between in situ validation measurements and
314   footprint average values [1]. More importantly, the results presented here give a
315   sense of how much variability is being captured by a given footprint. If one wanted
316   to capture scales of variability smaller than the mesoscale, that would mean a
317   smaller than ~50 km footprint in mid-latitude and smaller than ~20 km in the
318   tropics. In the tropics that varies by season as well.

319   **5. Conclusions**

320   From in situ data, it appears that at the SPURS-1 site, SFV is mainly generated
321   by internal ocean variability since its seasonality is unrelated to that of

precipitation in the region. SFV at SPURS-1 is highly seasonal, being largest in May-December and may be related to seasonality of the energy of the mesoscale eddy field. Assuming SFV is produced by the eddy field, it is scaled to the typical size of mesoscale variations, about 50-70 km.

At the SPURS-2 site, SFV is likely mostly produced by rainfall, whose scales are less than 20 km (Figure 5). It is also highly seasonal, with maximum values during the rainy (wet) season, June-January. At the scales examined, SFV showed little dependence on scale. The semivariograms examined in Figure 6 suggest that much of that dependence is contained within the shortest (<20 km) scales.

SFV is many times larger at the SPURS-2 site than at SPURS-1 (Figures 2, 3b and 4) at all footprint sizes. This highlights the fact that SFV is highly spatially dependent, and any accounting of the error associated with SFV needs to take that into account. There are very few areas in the open ocean that have been sampled as intensively for SSS as the SPURS regions. In order to get a full understanding of SFV error we must develop proxies which can stand in for the heavy sampling of the SPURS regions. We have attempted to do that here by examining two ROMS simulations. The one in the SPURS-1 region does a reasonable job of depicting the size and spatial dependence of SFV. In the SPURS-2 region, the simulation is less realistic, likely due to the lack of small-scale rainfall.

References

1.   Bingham, F.M. Subfootprint Variability of Sea Surface Salinity Observed during the SPURS-1 and SPURS-2 Field Campaigns. *Remote Sensing* **2019**, *11*, 2689, doi:10.3390/rs11222689.

2.   Boutin, J.; Chao, Y.; Asher, W.E.; Delcroix, T.; Drucker, R.; Drushka, K.; Kolodziejczyk, N.; Lee, T.; Reul, N.; Reverdin, G. Satellite and in situ salinity: understanding near-surface stratification and subfootprint variability. *Bulletin of the American Meteorological Society* **2016**, *97*, 1391-1407, doi:10.1175/BAMS-D-15-00032.1.

371   3.   Drushka, K.; Asher, W.E.; Sprintall, J.; Gille, S.T.; Hoang, C. Global patterns of submesoscale surface
372   salinity variability. *Journal of Physical Oceanography* **2019**, *49*, 1669-1685, doi:10.1175/JPO-D-19-0018.1.
373   4.   Lagerloef, G.S.; Colomb, F.R.; Le Vine, D.M.; Wentz, F.; Yueh, S.; Ruf, C.; Lilly, J.; Gunn, J.; Chao, Y.;
374   deCharon, A., et al. The Aquarius/SAC-D Mission: Designed to Meet the Salinity Remote-sensing
375   Challenge. *Oceanography* **2008**, *20*, 68-81.
376   5.   Abe, H.; Ebuchi, N. Evaluation of sea–surface salinity observed by Aquarius. *Journal of Geophysical*
377   *Research Oceans* **2014**, *119*, 8109-8121, doi:10.1002/2014JC010094.
378   6.   Kao, H.-Y.; Lagerloef, G.S.; Lee, T.; Melnichenko, O.; Meissner, T.; Hacker, P. Assessment of Aquarius Sea
379   Surface Salinity. *Remote Sensing* **2018**, *10*, 1341, doi:10.3390/rs10091341.
380   7.   Bao, S.; Wang, H.; Zhang, R.; Yan, H.; Chen, J. Comparison of Satellite-Derived Sea Surface Salinity
381   Products from SMOS, Aquarius, and SMAP. *Journal of Geophysical Research: Oceans* **2019**, *124*, 1932-1944,
382   doi:10.1029/2019jc014937.
383   8.   Fore, A.; Yueh, S.; Tang, W.; Hayashi, A. *SMAP Salinity and Wind Speed Users Guide, Version 4.3*; California
384   Institute of Technology: Pasadena, CA, 2020; p 259.
385   9.   Vinogradova, N.T.; Ponte, R.M. Small-scale variability in sea surface salinity and implications for
386   satellite-derived measurements. *Journal of Atmospheric and Oceanic Technology* **2013**, *30*, 2689-2694,
387   doi:10.1175/JTECH-D-13-00110.1.
388   10.   Jacobs, G.A.; Barron, C.N.; Rhodes, R.C. Mesoscale characteristics. *Journal of Geophysical Research* **2001**,
389   *106*, 19581-19595, doi:10.1029/2000JC000669.
390   11.   Kuragano, T.; Kamachi, M. Global statistical space-time scales of oceanic variability estimated from the
391   TOPEX/POSEIDON altimeter data. *Journal of Geophysical Research* **2000**, *105*, 955-974,
392   doi:10.1029/1999JC900247.
393   12.   Meyers, G.; Phillips, H.; Smith, N.; Sprintall, J. Space and time scales for optimal interpolation of
394   temperature — Tropical Pacific Ocean. *Progress in Oceanography* **1991**, *28*, 189-218, doi:10.1016/0079-
395   6611(91)90008-A.
396   13.   Bingham, F.M.; Lee, T. Space and time scales of sea surface salinity and freshwater forcing variability in
397   the global ocean (60° S–60° N). *Journal of Geophysical Research: Oceans* **2017**, *122*, 2909-2922,
398   doi:10.1002/2016JC012216.
399   14.   D'Addezio, J.M.; Bingham, F.M.; Jacobs, G.A. Sea surface salinity subfootprint variability estimates from
400   regional high-resolution model simulations. *Remote Sensing of Environment* **2019**, *233*, 111365, doi:10.1016/
401   j.rse.2019.111365.
402   15.   Drushka, K.; Asher, W.E.; Jessup, A.T.; Thompson, E.J.; Iyer, S.; Clark, D. Capturing Fresh Layers with the
403   Surface Salinity Profiler. *Oceanography* **2019**, *32*, doi:10.5670/oceanog.2019.215.
404   16.   Lindstrom, E., J.; Edson, J.B.; Schanze, J.J.; Shcherbina, A.Y. SPURS-2: Salinity Processes in the Upper-
405   Ocean Regional Study 2 – The Eastern Equatorial Pacific Experiment. *Oceanography* **2019**, *32*, doi:10.5670/
406   oceanog.2019.207.
407   17.   Lindstrom, E.; Bryan, F.; Schmitt, R. SPURS: Salinity Processes in the Upper-ocean Regional Study.
408   *Oceanography* **2015**, *28*, 14, doi:10.5670/oceanog.2015.01.
409   18.   Melnichenko, O.; Hacker, P.; Bingham, F.M.; Lee, T. Patterns of SSS Variability in the Eastern Tropical
410   Pacific: Intraseasonal to Interannual Timescales from Seven Years of NASA Satellite Data. *Oceanography*
411   **2019**, *32*, doi:10.5670/ oceanog.2019.208.
412   19.   Rutledge, S.A.; Chandrasekar, V.; Fuchs, B.; George, J.; Junyent, F.; Dolan, B.; Kennedy, P.C.; Drushka, K.
413   SEA-POL Goes to Sea. *Bulletin of the American Meteorological Society* **2019**, *100*, 2285-2301,
414   doi:10.1175/BAMS-D-18-0233.1.
415   20.   Rutledge, S., A.; Chandrasekar, V.; Fuchs, B.; George, J.; Junyent, F.; Kennedy, P.; Dolan, B. Deployment
416   of the SEA-POL C-band Polarimetric Radar to SPURS-2. *Oceanography* **2019**, *32*,
417   doi:10.5670/oceanog.2019.212.
418   21.   Farrar, J.T.; Rainville, L.; Plueddemann, A.J.; Kessler, W.S.; Lee, C.; Hodges, B.A.; Schmitt, R.W.; Edson,
419   J.B.; Riser, S.C.; Eriksen, C.C., et al. Salinity and temperature balances at the SPURS central mooring
420   during fall and winter. *Oceanography* **2015**, *28*, 56–65, doi:10.5670/oceanog.2015.06.
421   22.   Farrar, J.T.; Plueddemann, A.J. On the Factors Driving Upper-Ocean Salinity Variability at the Western
422   Edge of the Eastern Pacific Fresh Pool. *Oceanography* **2019**, *32*, doi:10.5670/oceanog.2019.209.
423   23.   Yu, L. On sea surface salinity skin effect induced by evaporation and implications for remote sensing of
424   ocean salinity. *Journal of Physical Oceanography* **2010**, *40*, 85-102.

425   24.   Centurioni, L.R.; Hormann, V.; Chao, Y.; Reverdin, G.; Font, J.; Lee, D.K. Sea Surface Salinity
426   Observations with Lagrangian Drifters in the Tropical North Atlantic During SPURS: Circulation, Fluxes,
427   and Comparisons with Remotely Sensed Salinity from Aquarius. *Oceanography* **2015**, *28*,
428   doi:10.5670/oceanog.2015.08.
429   25.   Doney, S.C.; Glover, D.M.; McCue, S.J.; Fuentes, M. Mesoscale Variability of Sea-Viewing Wide Field-of-
430   view Sensor (SeaWiFS) Satellite Ocean Color: Global Patterns and Spatial Scales. *Journal of Geophysical*
431   *Research* **2003**, *108*, 3024, doi:10.1029/2001JC000843.
432   26.   Clayson, C.A.; Edson, J.B.; Paget, A.; Graham, R.; Greenwood, B. Effects of Rainfall on the Atmosphere
433   and the Ocean During SPURS-2. *Oceanography* **2019**, *32*, doi:10.5670/oceanog.2019.216.
434   27.   Thompson, E., J.; Asher, W.E.; Jessup, A.T.; Drushka, K. High-Resolution Rain Maps from an X-band
435   Marine Radar and Their Use in Understanding Ocean Freshening. *Oceanography* **2019**, *32*,
436   doi:10.5670/oceanog.2019.213.
437   28.   Li, Z.; Bingham, F.M.; Li, P.P. Multiscale Simulation, Data Assimilation, and Forecasting in Support of the
438   SPURS-2 Field Campaign. *Oceanography* **2019**, *32*, doi:10.5670/oceanog.2019.221.
439   29.   Rainville, L.; Centurioni, L.R.; Asher, W.E.; Clayson, C.A.; Drushka, K.; Edson, J.B.; Hodges, B.A.;
440   Hormann, V.; Farrar, J.T.; Schanze, J.J., et al. Novel and Flexible Approach to Access the Open Ocean:
441   Uses of Sailing Research Vessel Lady Amber During SPURS-2. *Oceanography* **2019**, *32*,
442   doi:10.5670/oceanog.2019.219.
443   30.   Volkov, D., L.; Dong, S.; Foltz, G.R.; Goni, G.; Lumpkin, R. Observations of Near-Surface Salinity and
444   Temperature Structure with Dual-Sensor Lagrangian Drifters During SPURS-2. *Oceanography* **2019**, *32*,
445   doi:10.5670/oceanog.2019.214.
446   31.   Asher, W., E; Drushka, K.; Jessup, A.T.; Thompson, E.J.; Clark, D. Estimating Rain-Generated Turbulence
447   at the Ocean Surface Using the Active Controlled Flux Technique. *Oceanography* **2019**, *32*,
448   doi:10.5670/oceanog.2019.218.
449   32.   Delcroix, T.; Chaigneau, A.; Soviadan, D.; Boutin, J.; Pegliasco, C. Eddy-Induced Salinity Changes in the
450   Tropical Pacific. *Journal of Geophysical Research: Oceans* **2019**, *124*, 374-389, doi:10.1029/2018JC014394.
451

452